Available online at www.sciencedirect.com

ScienceDirect

journal homepage: www.elsevier.com/locate/he

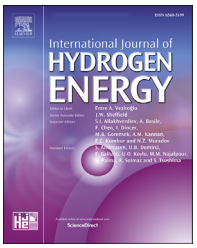

Investigation of structural, electronic and lattice dynamical properties of $XNiH_3$ (X = Li, Na and K) perovskite type hydrides and their hydrogen storage applications

Aysenur Gencer [a,b], *Gokhan Surucu* [a,c,d,*]

[a] *Department of Physics, Middle East Technical University, Turkey*
[b] *Department of Physics, Karamanoglu Mehmetbey University, Turkey*
[c] *Department of Electric and Energy, Ahi Evran University, Turkey*
[d] *Photonics Application and Research Center, Gazi University, Turkey*

ARTICLE INFO

Article history:
Received 19 January 2019
Received in revised form
7 April 2019
Accepted 10 April 2019
Available online 30 April 2019

Keywords:
Hydrogen storage
Perovskite type hydrides
Mechanical properties
Electronic properties
Thermodynamic properties

ABSTRACT

$XNiH_3$ (X = Li, Na, and K) perovskite type hydrides have been studied by using Density Functional Theory (DFT) and these materials are found to be stable and synthesizable. The X-ray diffraction patterns have been obtained and they indicate that all materials have the polycrystalline structure. The electronic properties have been investigated and it has been found that these structures show metallic character. The Bader partial charge analysis has also been performed. In addition, the elastic constants have been calculated and these materials are found to be mechanically stable. Using these elastic constants, the mechanical properties such as bulk modulus, shear modulus, Poisson's ratio have been obtained. Moreover, the Debye temperatures and thermal conductivities have been studied. The anisotropic elastic properties have been visualized in three dimensions (3D) for Young's modulus, linear compressibility, shear modulus and Poisson's ratio as well as with the calculation of the anisotropic factors. Additionally, the dynamical stability has been investigated and obtained phonon dispersion curves show that these materials are dynamically stable. Also, the thermal properties including free energy, enthalpy, entropy and heat capacity have been studied. The hydrogen storage properties have been examined and the gravimetric hydrogen storage capacities have been calculated as 4.40 wt%, 3.57 wt % and 3.30 wt% for $LiNiH_3$, $NaNiH_3$ and $KNiH_3$, respectively. Furthermore, the hydrogen desorption temperatures have been obtained as 446.3 K, 419.5 K and 367.5 K for $LiNiH_3$, $NaNiH_3$ and $KNiH_3$, respectively.

© 2019 Hydrogen Energy Publications LLC. Published by Elsevier Ltd. All rights reserved.

* *Corresponding author*. Ahi Evran University, Department of Electric and Energy, 40100, Kirsehir, Turkey.
E-mail address: g_surucu@yahoo.com (G. Surucu).

https://doi.org/10.1016/j.ijhydene.2019.04.097

0360-3199/© 2019 Hydrogen Energy Publications LLC. Published by Elsevier Ltd. All rights reserved.

Introduction

The technological development affects the daily life in modern societies which causes more energy demand. Currently, the most used energy source is fossil fuels that are limited. Also, these sources release greenhouse gases that contributes to global warming. Moreover, the world's energy demand increases more than 25% between today and 2040 according to the International Energy Agency New Policies Scenario [1]. Therefore, new energy sources have to be explored. One of the possible energy sources is hydrogen which is the most abundant element on the Earth. In addition, the water is produced after combustion of hydrogen. The mass energy content of hydrogen is three times higher than gasoline while the volume energy content is four times lower than gasoline [2]. Also, the efficiency of hydrogen is higher than gasoline in the fuel cells [2]. In view of these properties of hydrogen, the new energy scenarios could include a hydrogen economy [3] which includes production, storage and use. This study focuses on hydrogen storage.

Hydrogen storage methods are classified into three: gas, liquid and solid state storage [4,5]. Hydrogen is a gas at ambient conditions. Therefore, the gas hydrogen storage method requires high pressure vessels that demand safety cautions [6]. For liquid hydrogen storage method, hydrogen must be liquefied that needs additional energy and cryogenic temperatures [6]. Also, boiling of hydrogen should be considered for this method. Solid state hydrogen storage methods could divide into two categories, physisorption of hydrogen and chemisorption of hydrogen [4]. For the physisorption, hydrogen is bonded to the surface of a material and generally high surface area carbon, carbon nanotubes and zeolites have been studied [7]. For the chemisorption, hydrogen has chemical bonds with a material and metal hydrides and complex hydrides are the commonly studied materials [6–11]. The one of the most considered metal hydride is MgH_2 compound that has high hydrogen storage capacity with low hydrogen desorption kinetics. Besides MgH_2, magnesium borohydride with $Mg(BH_4)_2$ formula has a high hydrogen storage capacity as 14.94 wt% [12]. Also, several studies have been performed with Mg and transitions metals that have relatively low storage capacity but good kinetics [13–15]. Recently, the dopants to MgH_2 have been investigated and it has been found that the dopants improve the hydrogen desorption kinetics of MgH_2 [16–21]. Also, the reaction of two or more hydrides have been investigated that enhance the hydrogen kinetics for desorption and absorption [22,23]. Furthermore, another promising material group are Nickel-based hydrides for the reversible hydrogen storage with stability and appropriate kinetics [10,24–26].

In this study, perovskite type hydrides have been investigated which is one of the material group for the solid-state hydrogen storage method. Perovskite type hydrides with ABH_3 formula, have high gravimetric hydrogen storage capacities [27]. The possible combinations for the perovskite type hydrides are $A^{+1}B^{+2}H_3^{-1}$ and $A^{+2}B^{+1}H_3^{-1}$. Hence, there are limited number of perovskite type hydrides due to generally composing from 1A to 2A group elements. The most studied perovskite type hydride is $NaMgH_3$ [28–30]. In the literature, $LiNiH_3$ perovskite type hydride has been synthesized and investigated using in situ synchrotron X-ray diffraction [31] and also theoretical modeling [32]. The investigation of $LiNiH_3$ is interesting due to having Nickel, an 8B group element.

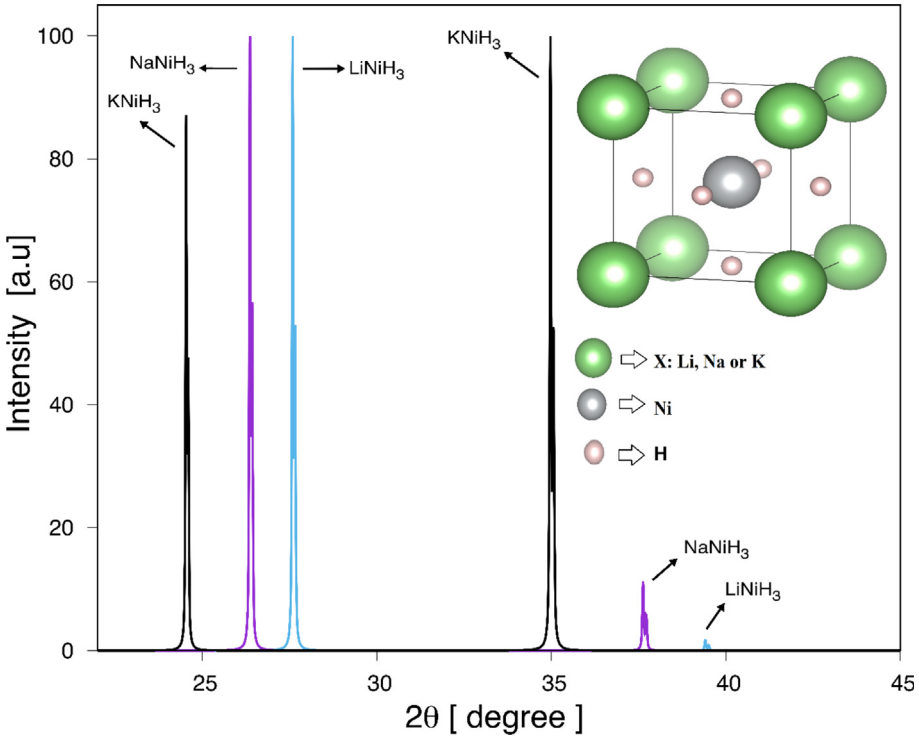

Fig. 1 – The X-ray diffraction pattern and the crystal structure for $XNiH_3$.

Table 1 – The lattice parameters (a in Å), densities (ρ in g/cm^3), scattering angles (2θ), and formation energies (ΔE_f in eV/atom) for $XNiH_3$.

Compound		a	ρ	2θ	ΔE_f
$LiNiH_3$	This work	3.23	3.38	27.59	−0.73
	Exp. [12]	3.21			
	Theory [13]	3.25			
$NaNiH_3$	This work	3.28	3.65	26.37	−0.69
$KNiH_3$	This work	3.62	3.51	24.54	−0.61

With the inspiration from these studies, $XNiH_3$ ($X = Li$, Na, and K) have been studied in order to examine their hydrogen storage properties using Density Functional Theory (DFT). In addition, the effect of the change of X element in the compounds have been discussed in detail.

Calculation details

The Vienna Ab-initio Simulation Package (VASP) [33,34] has been employed for DFT calculations. The Perdew-Burke-Ernzerhof (PBE) functional [35] has been used for the exchange correlation term of the electron-electron interaction within the Generalized Gradient Approximation (GGA). For the electron-ion interaction, Projector Augmented Wave (PAW) [36,37] method has been chosen with a kinetic energy cut offs as 600 eV for $LiNiH_3$ and 550 eV for $NaNiH_3$ and $KNiH_3$. In addition, the k-points have been obtained with a gamma centered mesh [38] that yields a 12 × 12 × 12 k-points. The energy tolerance criterion has been chosen as 10^{-10} eV per unit cell for the solution of the Kohn-Sham equations. The force convergence has been performed with a criterion as 10^{-9} eV/Å for the minimization of the stresses and the Hellman-Feynman forces. The Bader partial charge calculations have been performed using VASP and the analysis has been done using algorithm developed by Henkelman et al. [39] that is based on Bader's suggestion [40]. Also, the elastic constants have been studied using stress-strain method that is implemented in VASP [41]. For the vibrational properties, PHONOPY software [42] has been used for the supercell generation and this supercell has been employed to VASP using linear response method. Additionally, X-ray diffraction patterns are obtained by using VESTA program package [43] and the Cu Ka source having the wavelength of 1.541 Å is used.

Results and discussions

Structural and hydrogen storage properties

The $XNiH_3$ ($X = Li$, Na, *and* K) perovskite type hydrides have been optimized in the cubic phase (Pm-3m (space group: 221)) and their X-ray diffraction pattern and the crystal structures are shown in Fig. 1. The structural parameters (lattice parameters (a in Å), densities (ρ in g/cm^3), and the scattering angles (2θ) for (1 0 0) direction) have been listed in Table 1. The optimized lattice parameters for $LiNiH_3$ is consistent with the available experimental [12] and theoretical [13] studies as deduced from Table 1. However, there is no study in the literature for $NaNiH_3$ and $KNiH_3$ to compare the obtained results as known up to date. In addition, X-ray diffraction patterns of these materials indicate that these materials have explicit picks. So, these materials have polycrystalline property.

The formation energies (ΔE_f in eV/atom) have been calculated using Eq. (1). All compounds have negative formation energies which imply that these compounds are energetically stable and synthesizable compounds. The stability of these compounds has the order as $LiNiH_3 > NaNiH_3 > KNiH_3$.

$$\Delta Ef = E_t(XNiH_3) - [E(X) + E(Ni) + 3{*}E(H)] \quad (1)$$

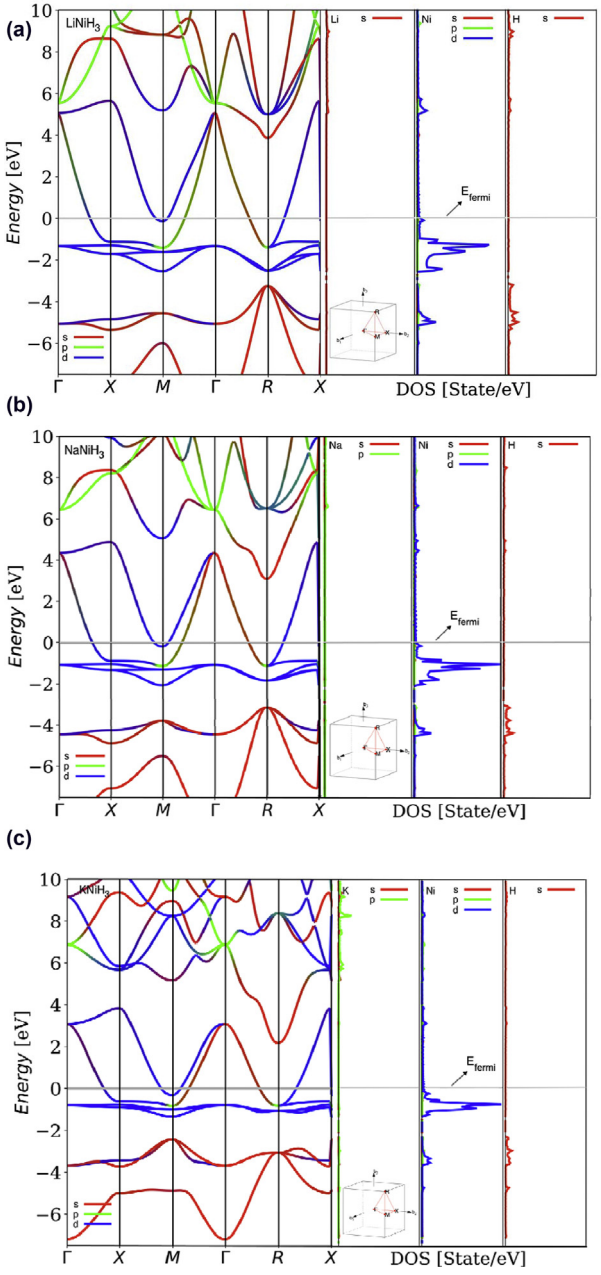

Fig. 2 – Band structures and partial density of states for (a) $LiNiH_3$, (b) $NaNiH_3$ and (c) $KNiH_3$.

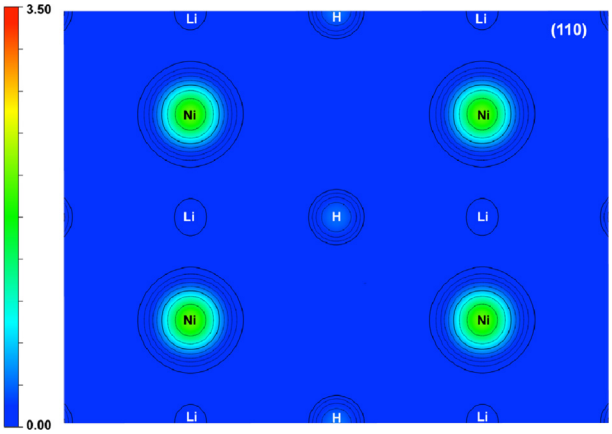

Fig. 3 – Electron-density distribution of $LiNiH_3$ for a 2 × 2 × 2 supercell.

Table 2 – Bader partial net charges (in units of e) for $XNiH_3$.

Atom	$LiNiH_3$	$NaNiH_3$	$KNiH_3$
Li, Na or K	0.88	0.80	0.70
Ni	0.21	0.30	0.39
H	−1.09	−1.10	−1.09

Electronic properties

The band structures and corresponding partial density of states (PDOS) have been obtained along the high symmetry points in the first Brillioun zone using the optimized structures for $XNiH_3$. Fig. 2 shows the band structures and PDOS where all compounds have metallic character. Also, Ni-based hydrides [10,24–26] show metallic character. So, it can be concluded that Ni atoms contribute the metallic character of the compounds. The contributions from electrons at the s (in red), p (in green) and d (in blue) orbitals to the band structures are illustrated with different colors in the figures. For $LiNiH_3$, there is a hybridization between electrons at the s orbitals of H and electrons at the d orbitals of Ni around −5 eV energy range. Similar behaviors have been seen around −4 eV for $NaNiH_3$ and $KNiH_3$. In addition, the most significant contribution at the Fermi level comes from the d states of *Ni*. Also, the path of the high symmetry points is inserted in the figures.

Fig. 3 shows the electron-density distribution for $LiNiH_3$ compound along (1 1 0) direction and $LiNiH_3$ has ionic bonding as can be seen from the figure. Charge densities of $NaNiH_3$ and $KNiH_3$ compounds have not been presented here in order to save space in the journal. In addition, to determine the charge of each ion in the structures, the Bader partial charge analysis have been performed and Table 2 lists the Bader net partial charges where the total Bader net charge is zero. The positive Bader charge implies that the charge is transferred away from the atom while the negative Bader charge implies that the charge is transferred to the atom [44]. The *X* and *Ni* atoms give charges away while *H* atoms take charge. The Bader net partial charges are similar for these compounds.

Table 4 – The longitudinal (V_l in m/s), transverse (V_t in m/s) and average wave velocities (V_m in m/s), Debye temperature (Θ_D in K), anisotropic factor A for $XNiH_3$.

Compound	V_l	V_t	V_m	Θ_D	A
$LiNiH_3$	7383	4331	4801	756.5	0.512
$NaNiH_3$	6871	4178	4616	695.6	0.857
$KNiH_3$	6122	3657	4047	568.3	1.792

Mechanical and anisotropic elastic properties

The elastic constants (C_{ij}) should be obtained in order to determine the mechanical stability of a material which is an important consideration for the technological applications. So, the elastic constants have been calculated using stress-strain method implemented in VASP. The necessary elastic constants for the cubic structures are C_{11}, C_{12} and C_{44} given in Table 3 for $XNiH_3$. The calculated constants satisfy the well-known Born stability criteria [45,46] given in Eq. (4). As a result, these compounds are mechanically stable and their mechanical properties could be further investigated.

$$C_{11} > 0, C_{44} > 0, C_{11} - C_{12} > 0, C_{11} + 2C_{12} > 0 \quad (2)$$

The calculated elastic constants could be used to determine some physical properties such as bulk modulus, shear modulus, etc. Table 3 lists these determined properties. The bulk and shear moduli have been determined using Voigt [47], Reuss [48], Hill [49] approximation. The result of Voigt approximation gives the highest limit for that modulus while the result of Reuss approximation gives the lowest limit. Also, the result of Hill approximation is generally more close to the experimental results. The values given in Table 3 are the results of the Hill approximation. Bulk modulus (B) is the resistance to volume change when a pressure is applied. $LiNiH_3$ has the highest bulk modulus as can be seen from Table 3. The shear modulus (G) is the ratio of the shear stress to shear strain. From Table 3, it can be concluded that $LiNiH_3$ and $NaNiH_3$ has close shear moduli while $KNiH_3$ has lower shear modulus. Young's modulus (E) also called modulus of elasticity is the ratio of the uniaxial stress to strain. Among the studied materials, $LiNiH_3$ has the highest Young's modulus. Poisson's ratio (ν) could be used to determine the bonding

Table 3 – The elastic constants (C_{ij} in GPa), bulk modulus (B in GPa), shear modulus (G in GPa), Young's modulus (E in GPa), Poisson's ratio (ν), G/B, and B/G ratios for $XNiH_3$.

Compound	C_{11}	C_{12}	C_{44}	B	G	E	ν	G/B	B/G
$LiNiH_3$	226.0	36.7	48.5	99.8	63.5	157.1	0.238	0.636	1.571
$NaNiH_3$	180.5	40.7	59.9	87.3	63.7	153.7	0.207	0.729	1.370
$KNiH_3$	113.2	46.9	59.4	69.0	47.0	114.9	0.222	0.681	1.468

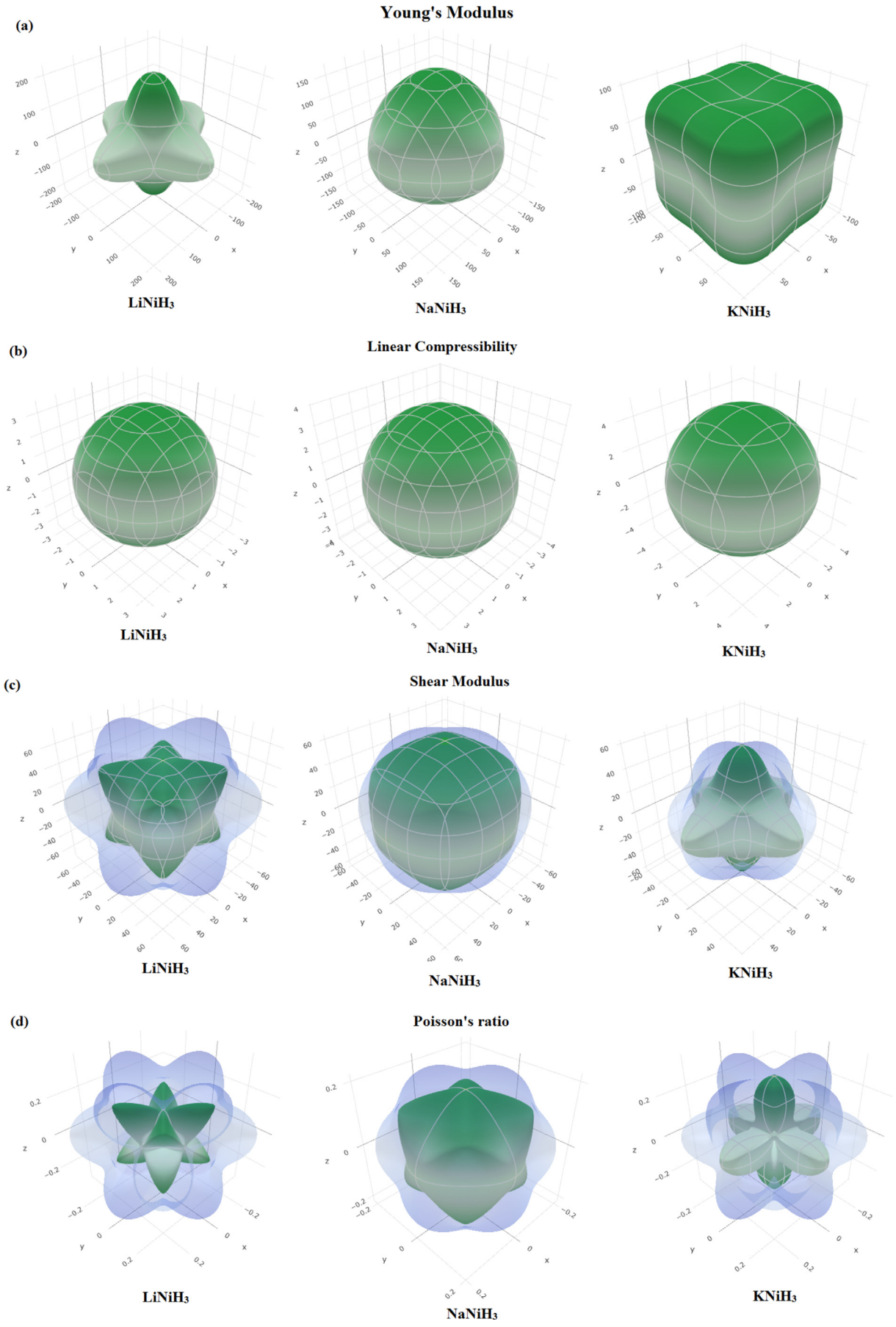

Fig. 4 – The directional dependent (a) Young's modulus, (b) linear compressibility, (c) shear modulus and (d) Poisson's ratio for $XNiH_3$.

Table 5 – The maximum and minimum values of the Young's modulus E (in GPa), linear compressibility β (in TPa^{-1}), shear modulus G (in GPa) and Poisson's ratio ν for $XNiH_3$.

Compound	E (GPa)		β (TPa^{-1})		G (GPa)		ν	
	E_{min}	E_{max}	β_{min}	β_{max}	G_{min}	G_{max}	ν_{min}	ν_{max}
$LiNiH_3$	125.22	215.75	3.34	3.34	48.50	94.65	0.09	0.44
$NaNiH_3$	146.25	165.52	3.82	3.82	59.90	69.90	0.17	0.26
$KNiH_3$	85.72	138.47	4.83	4.83	33.15	59.40	0.01	0.41

nature of a material. It is the measure of the expansion or contraction in the perpendicular directions to the direction of a compression or a stretching. If the Poisson's ratio is around 0.1, the material has dominantly covalent bonding, while if it is around 0.25, it has dominantly ionic bonding [50]. The studied compounds have the Poisson's ratio around 0.25, so they have dominantly ionic bonding. This result is consistent with the charge density distributions for these materials. The G/B ratio also called Pugh's modulus given in Table 3, could also be used to determine the bonding nature of a material. If G/B ratio is around 0.6, the dominant bonding is ionic and if it is 1.1, this time the dominant bonding is covalent [51]. The G/B ratios of the studied materials are around 0.6 that indicates that the ionic bonding is dominant consistent with the Poisson's ratio. The brittle or ductile nature of a material could be confirmed using B/G ratio. The brittle materials have B/G ratio lower than 1.75 while the ductile materials have higher than 1.75 [52]. The studied materials are brittle having the B/G ratios lower than 1.75.

For the next consideration of these materials, the Debye temperature and anisotropic elastic properties have been determined. The Debye temperature is related to some physical properties such as specific heat and melting temperature. A high value of the Debye temperature indicates that a high thermal conductivity and a high melting temperature for that material. The obtained longitudinal, transverse, average wave velocities, the Debye temperatures and anisotropic factors are listed in Table 4. The Debye temperature (Θ_D), average wave velocity (V_m), the longitudinal wave velocity (V_l) and the transverse (V_t) wave velocity have been calculated using below equations [53,54]. In Eq. (5), h is the Planck's constant, k is the Boltzman's constant, n is the number of atoms per formula unit, ρ is the density, M is the mass of atoms contained in the unit cell and N_A is the Avogadro number.

$$\Theta_D = \frac{h}{k}\left[\frac{3n}{4\pi}\frac{N_A\rho}{M}\right]^{1/3} V_m \tag{3}$$

$$V_m = \left[\frac{1}{3}\left(\frac{2}{V_t^3} + \frac{1}{V_l^3}\right)\right]^{-1/3} \tag{4}$$

$$V_t = \sqrt{\frac{G}{\rho}} \tag{5}$$

$$V_l = \sqrt{\frac{3B + 4G}{3\rho}} \tag{6}$$

$LiNiH_3$ has the highest Debye temperature. When X atom changes from Li to K, both the wave velocities and the Debye temperature decrease. The anisotropic factors are important for the technological considerations. Eq. (7) [55] have been used for the calculation of the anisotropic factors and obtained A values are given in Table 4. For the cubic crystal structures A_1, A_2 and A_3 are equal due to the crystal symmetry. If the anisotropic factor is equal to one, this implies that the material is isotropic while it is lower or higher than one, this implies the anisotropy. Both compounds have anisotropy.

$$A1 = A2 = A3 = A = \frac{2C_{44}}{(C_{11} - C_{12})} \tag{7}$$

In addition to anisotropic factors, the anisotropic elastic properties have been visualized in 3D using ELATE software [56]. The anisotropic elastic factors give an information about the material properties in specific directions. Fig. 4 shows the directional dependent Young's modulus, linear compressibility, shear modulus and Poisson's ratio for $XNiH_3$. The green shapes show the minimum for that parameter while blue shapes show the maximum. For the isotropic materials, the shape is spherical and distortion from the spherical shape indicates the anisotropy. Only linear compressibility is isotropic. Young's modulus, shear modulus and Poisson's ratio are anisotropic. Furthermore, the maximum and minimum values for these parameters are listed in Table 5.

Vibrational and thermodynamic properties

The dynamical stability of a compound could be determined with the phonon dispersion curves. The generated 2 × 2 × 2 supercells for these compounds have been employed to VASP and the phonon dispersion curves have been calculated using linear response method. Fig. 5 shows the phonon dispersion curves and phonon density of states for $XNiH_3$. The unit cell of $XNiH_3$ has five atoms and as a result there are 15 phonon branches in the figures where three of them are acoustic and the remaining are optic branches. As can be seen from the figures, there are no soft modes. Therefore, these compounds are dynamically stable materials. Also, *H* being the lightest element in the compounds, gives contributions to the higher frequencies that is the expected situation. In addition, the zero point energies (E_{ZPE}) for these compounds could be obtained from the phonon studies. The obtained zero point energies are 0.62 eV, 0.63 eV and 0.54 eV for $LiNiH_3$, $NaNiH_3$ and $KNiH_3$, respectively.

In addition, when *X* atom changes from *Li* to *K*, the frequencies of the acoustic and optic branches are close to each other that is related to the lower thermal conductivities. This condition is consistent with the results given in Table 6. The minimum thermal conductivities for these materials have been obtained using two models: Clarke's model [57] and

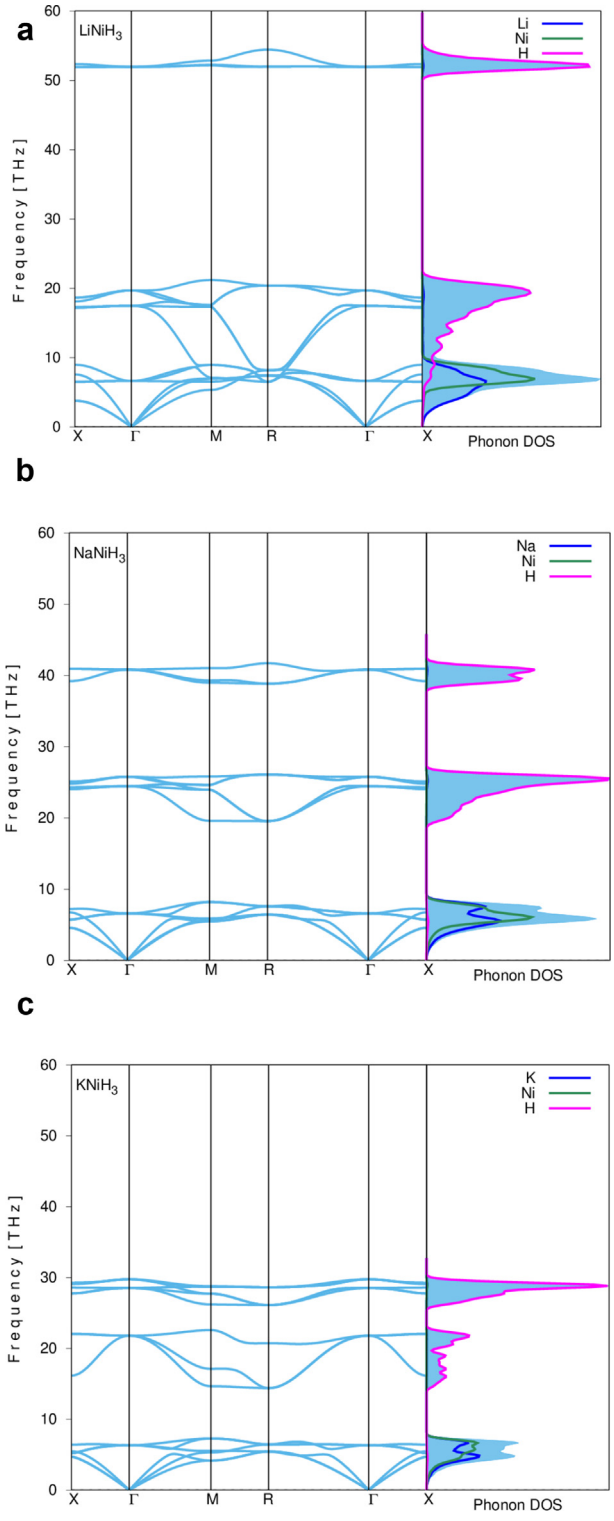

Fig. 5 – The phonon dispersion curves and phonon density of states for (a) $LiNiH_3$, (b) $NaNiH_3$ and (c) $KNiH_3$.

Cahill's model [58]. M_a is the average mass per atom and n is the density of number of atoms per volume. The minimum thermal conductivities (λ_{min}) decrease when the *X* atom changes from *Li* to *K*.

Table 6 – The lower limits of thermal conductivities using Clarke's and Cahill models for $XNiH_3$.

Compound	Clarke's model		Cahill's model	
	M_a (10^{-26} kg)	λ_{min} (W m^{-1} K^{-1})	n (10^{28} m^{-3})	λ_{min} (W m^{-1} K^{-1})
$LiNiH_3$	2.282	2.293	14.800	2.503
$NaNiH_3$	2.812	1.998	12.900	2.172
$KNiH_3$	3.347	1.528	10.400	1.665

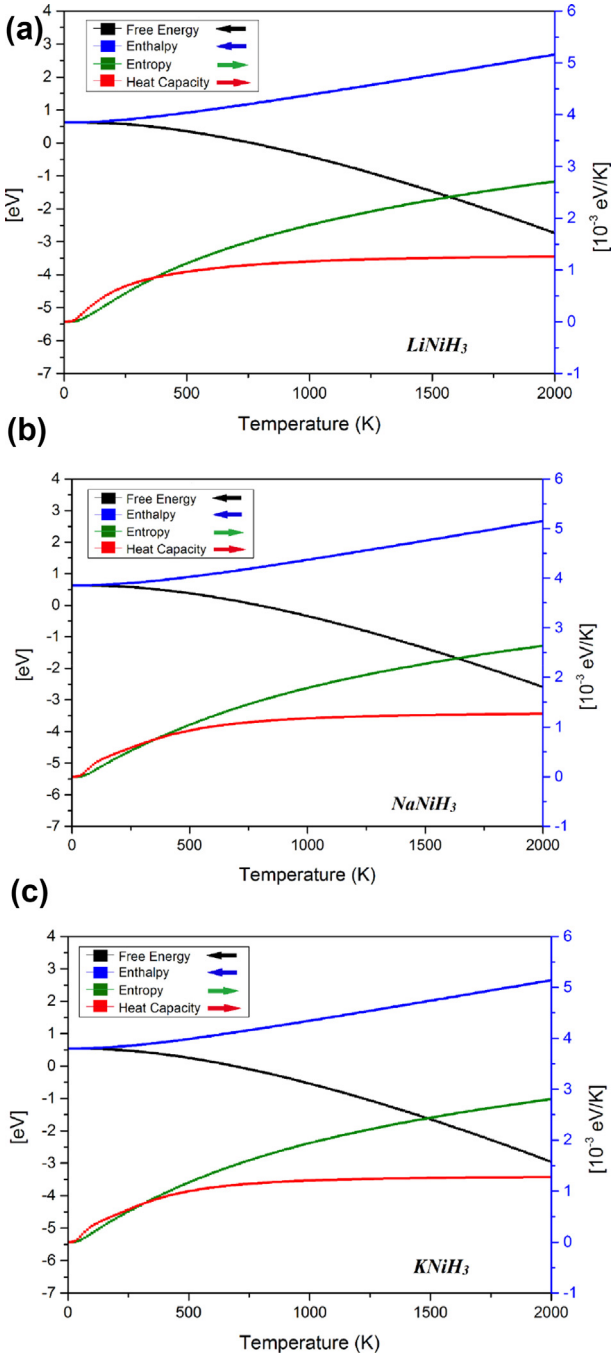

Fig. 6 – The free energy, enthalpy, entropy and heat capacity as a function of temperature for (a) $LiNiH_3$, (b) $NaNiH_3$ and (c) $KNiH_3$.

Table 7 – The gravimetric hydrogen storage capacity ($C_{wt\%}$) and hydrogen desorption temperature (T in K) for $XNiH_3$.

Compound	$C_{wt\%}$	T
$LiNiH_3$	4.40	446.3
$NaNiH_3$	3.57	419.5
$KNiH_3$	3.30	367.5

The thermal properties (free energy, enthalpy, entropy, and heat capacity) of $XNiH_3$ have been obtained using phonon information and quasi harmonic Debye model [42] as shown in Fig. 6. As the temperature increases, the enthalpy and the entropy increase while the free energy decreases. Also, the heat capacity reaches a constant called the Dulong-Petit limit at high temperatures.

Hydrogen storage properties

The hydrogen storage properties (gravimetric hydrogen storage capacity and hydrogen desorption temperature) of these compounds have to be studied to discuss their applications in this field. The gravimetric hydrogen storage capacity is the amount of hydrogen stored per unit mass of a material. Table 7 lists the gravimetric hydrogen storage capacities for the studied compounds that are calculated using Eq. (8) [10]. H/M is the hydrogen to material atom ratio, M_H is the molar mass of hydrogen and M_{Host} is the molar mass of the host material. When the *X* atom changes from *Li* to *K*, the gravimetric hydrogen storage capacity decreases to due to increasing of the mass of the compound. The obtained results are compared with the Ni-based compounds such as $LaMgNiH_4$ [10] and Mg_2NiH_6 [4]. The gravimetric hydrogen storage capacities are 1.74 wt% and 3.59 wt% for $LaMgNiH_4$ and Mg_2NiH_6, respectively. So, the studied compounds have significant storage capacities.

$$C_{wt\%} = \left(\frac{\left(\frac{H}{M}\right) M_H}{M_{Host} + \left(\frac{H}{M}\right) M_H} \times 100 \right) \% \tag{8}$$

Another essential parameter is the hydrogen desorption temperature for the hydrogen storage applications. The hydrogen desorption temperature is the required temperature to release the stored hydrogen. The obtained hydrogen desorption temperatures are listed in Table 7 as well. These temperatures have been calculated using Eq. (9) at 1 bar pressure where ΔH is the obtained formation enthalpy and ΔS is the entropy change of hydrogen that is 130 kJ/mol K [59]. The zero-point energy correction contributes the formation enthalpy that has been calculated from Eq. (1). The corrected formation enthalpy could be obtained using Eq. (10) [60] and Δ E_{ZPE} are the zero point energies given in Section Vibrational and thermodynamic properties.

$$\Delta H = T \times \Delta S \tag{9}$$

$$\Delta E_f^{cor} = \Delta E_f + \Delta E_{ZPE} \tag{10}$$

The hydrogen desorption temperature decreases when the *X* atom changes from *Li* to *K*. Once the results are compared with Mg_2NiH_6 [4] having the hydrogen desorption temperature as 555 K, it has been deduced that the obtained temperatures are lower than that of the Ni-based hydrides. In addition, if one needs to lower desorption temperatures despite of lower hydrogen storage capacity, $KNiH_3$ is an option or the high hydrogen storage capacity is crucial despite the high desorption temperature, this time $LiNiH_3$ is an option with these considerations.

Conclusion

In this study, $XNiH_3$ where *X* is *Li*, *Na* or *K* perovskite type hydrides have been investigated and these compounds are found to be energetically, mechanically and dynamically stable and synthesizable. The band structures show that these compounds have metallic character. In addition, the Bader partial charge analysis reveals that *X* and *Ni* atoms give charges away while *H* atoms take charge. These compounds have dominantly ionic bonding that has been determined from the Poisson's ratio and G/B ratio. The B/G ratios for these materials show that they are brittle materials. Also, $NaNiH_3$ is found to be as the hardest material among the studied compounds. In addition, the free energy, enthalpy, entropy and heat capacity have been investigated as a function of temperature and it has been found that enthalpy and entropy increase when the temperature increases while free energy decreases. The hydrogen storage properties have been investigated and it is deduced that $LiNiH_3$ has the highest gravimetric hydrogen storage capacity and the hydrogen desorption temperature (4.40 wt%, 446.3 K) while $KNiH_3$ has the lowest ones (3.30 wt%, 367.5 K). Consequently, the theoretical predictions on the $XNiH_3$ (*X* = *Li*, *Na* or *K*) perovskite type hydrides would be serving as a reliable reference for the future experimental and theoretical studies.

Acknowledgments

This work was supported by the Ahi Evran University Research Project Unit under Project No PYO-KMY.4001.15.001.

REFERENCES

[1] Agency IE. World energy outlook. 2018. n.d, https://www.iea.org/weo2018/. [Accessed 14 December 2018].
[2] Niaz S, Manzoor T, Pandith AH. Hydrogen storage: materials, methods and perspectives. Renew Sustain Energy Rev 2015;50:457–69. https://doi.org/10.1016/J.RSER.2015.05.011.
[3] Crabtree GW, Dresselhaus MS, Buchanan MV. The hydrogen economy. Phys Today 2004;57:39–44. https://doi.org/10.1063/1.1878333.
[4] WALKER G. Hydrogen storage technologies. Solid-State Hydrog Storage 2008:3–17. https://doi.org/10.1533/9781845694944.1.3.
[5] Schlapbach L, Züttel A. Hydrogen-storage materials for mobile applications. Nature 2001;414:353–8. https://doi.org/10.1038/35104634.
[6] Sakintuna B, Lamari-Darkrim F, Hirscher M. Metal hydride materials for solid hydrogen storage: a review. Int J Hydrogen Energy 2007;32:1121–40. https://doi.org/10.1016/J.IJHYDENE.2006.11.022.

[7] Eberle U, Felderhoff M, Schüth F. Chemical and physical solutions for hydrogen storage. Angew Chem Int Ed 2009;48:6608–30. https://doi.org/10.1002/anie.200806293.
[8] Jain IP, Jain P, Jain A. Novel hydrogen storage materials: a review of lightweight complex hydrides. J Alloy Comp 2010;503:303–39. https://doi.org/10.1016/J.JALLCOM.2010.04.250.
[9] Jena P. Materials for hydrogen storage: past, present, and future. J Phys Chem Lett 2011;2:206–11. https://doi.org/10.1021/jz1015372.
[10] Baysal MB, Surucu G, Deligoz E, Ozısık H. The effect of hydrogen on the electronic, mechanical and phonon properties of LaMgNi4 and its hydrides for hydrogen storage applications. Int J Hydrogen Energy 2018;43:23397–408. https://doi.org/10.1016/J.IJHYDENE.2018.10.183.
[11] Zarshenas M, Ahmed R, Kanoun MB, ul Haq B, Mat Isa AR, Goumri-Said S. First principle investigations of the physical properties of hydrogen-rich MgH_2. Phys Scripta 2013;88:065704. https://doi.org/10.1088/0031-8949/88/06/065704.
[12] Goumri-Said S, Ahmed R, Kanoun MB. Density-functional theory study of high hydrogen content complex hydrides Mg(BH4)2 at low temperature. Renew Energy 2016;90:114–9. https://doi.org/10.1016/J.RENENE.2015.12.044.
[13] Ul Haq B, Kanoun MB, Ahmed R, Bououdina M, Goumri-Said S. Hybrid functional calculations of potential hydrogen storage material: complex dimagnesium iron hydride. Int J Hydrogen Energy 2014;39:9709–17. https://doi.org/10.1016/J.IJHYDENE.2014.04.014.
[14] Li Y, Yang J, Luo L, Hu F, Zhai T, Zhao Z, et al. Microstructure characteristics, hydrogen storage kinetic and thermodynamic properties of Mg80–xNi20Yx (x = 0–7) alloys. Int J Hydrogen Energy 2019;44:7371–80. https://doi.org/10.1016/J.IJHYDENE.2019.01.216.
[15] Zhang Y, Li X, Cai Y, Qi Y, Guo S, Zhao D. Improved hydrogen storage performances of Mg-Y-Ni-Cu alloys by melt spinning. Renew Energy 2019;138:263–71. https://doi.org/10.1016/J.RENENE.2019.01.106.
[16] Yahya MS, Sulaiman NN, Mustafa NS, Halim Yap FA, Ismail M. Improvement of hydrogen storage properties in MgH2 catalysed by K2NbF7. Int J Hydrogen Energy 2018;43:14532–40. https://doi.org/10.1016/J.IJHYDENE.2018.05.157.
[17] Wang K, Wu G, Cao H, Li H, Zhao X. Improved reversible dehydrogenation properties of MgH2 by the synergetic effects of graphene oxide-based porous carbon and TiCl3. Int J Hydrogen Energy 2018;43:7440–6. https://doi.org/10.1016/J.IJHYDENE.2018.02.195.
[18] Sazelee NA, Idris NH, Md Din MF, Mustafa NS, Ali NA, Yahya MS, et al. Synthesis of BaFe12O19 by solid state method and its effect on hydrogen storage properties of MgH2. Int J Hydrogen Energy 2018;43:20853–60. https://doi.org/10.1016/J.IJHYDENE.2018.09.125.
[19] Yahya MS, Ismail M. Synergistic catalytic effect of SrTiO3 and Ni on the hydrogen storage properties of MgH2. Int J Hydrogen Energy 2018;43:6244–55. https://doi.org/10.1016/J.IJHYDENE.2018.02.028.
[20] Pighin SA, Coco B, Troiani H, Castro FJ, Urretavizcaya G. Effect of additive distribution in H2 absorption and desorption kinetics in MgH2 milled with NbH0.9 or NbF5. Int J Hydrogen Energy 2018;43:7430–9. https://doi.org/10.1016/J.IJHYDENE.2018.02.151.
[21] Ismail M, Mustafa NS, Ali NA, Sazelee NA, Yahya MS. The hydrogen storage properties and catalytic mechanism of the CuFe2O4-doped MgH2 composite system. Int J Hydrogen Energy 2019;44:318–24. https://doi.org/10.1016/j.ijhydene.2018.04.191.
[22] Mustafa NS, Halim Yap FA, Yahya MS, Ismail M. The hydrogen storage properties and reaction mechanism of the NaAlH4 + Ca(BH4)2 composite system. Int J Hydrogen Energy 2018;43:11132–40. https://doi.org/10.1016/J.IJHYDENE.2018.04.234.
[23] Halim Yap FA, Mustafa NS, Yahya MS, Mohamad AA, Ismail M. A study on the hydrogen storage properties and reaction mechanism of Na3AlH6LiBH4 composite system. Int J Hydrogen Energy 2018;43:8365–74. https://doi.org/10.1016/J.IJHYDENE.2018.03.070.
[24] Ćirić KD, Koteski VJ, Stojić DL j, Radakovic JS, Ivanovski VN. HfNi and its hydrides – first principles calculations. Int J Hydrogen Energy 2010;35:3572–7. https://doi.org/10.1016/J.IJHYDENE.2010.01.127.
[25] Chattaraj D, Dash S, Majumder C. Structural, electronic, elastic, vibrational and thermodynamic properties of ZrNi and ZrNiH3: a comprehensive study through first principles approach. Int J Hydrogen Energy 2016;41:20250–60. https://doi.org/10.1016/J.IJHYDENE.2016.09.046.
[26] Bouhadda Y, Rabehi A, Boudouma Y, Fenineche N, Drablia S, Meradji H. Hydrogen solid storage: first-principles study of ZrNiH3. Int J Hydrogen Energy 2009;34:4997–5002. https://doi.org/10.1016/J.IJHYDENE.2008.12.082.
[27] Ikeda K, Sato T, Orimo S. Perovskite-type hydrides – synthesis, structures and properties. Int J Mater Res 2008;99:471–9. https://doi.org/10.3139/146.101671.
[28] Wu H, Zhou W, Udovic TJ, Rush JJ, Yildirim T. Crystal chemistry of perovskite-type hydride $NaMgH_3$: implications for hydrogen storage. Chem Mater 2008;20:2335–42. https://doi.org/10.1021/cm703356v.
[29] Ikeda K, Kato S, Shinzato Y, Okuda N, Nakamori Y, Kitano A, et al. Thermodynamical stability and electronic structure of a perovskite-type hydride, NaMgH3. J Alloys Comp 2007;446–447:162–5. https://doi.org/10.1016/J.JALLCOM.2007.03.093.
[30] Bouhadda Y, Bououdina M, Fenineche N, Boudouma Y. Elastic properties of perovskite-type hydride NaMgH3 for hydrogen storage. Int J Hydrogen Energy 2013;38:1484–9. https://doi.org/10.1016/J.IJHYDENE.2012.11.047.
[31] Sato R, Saitoh H, Endo N, Takagi S, Matsuo M, Aoki K, et al. Formation process of perovskite-type hydride $LiNiH_3$: *in situ* synchrotron radiation X-ray diffraction study. Appl Phys Lett 2013;102:091901. https://doi.org/10.1063/1.4794067.
[32] Takagi S, Saitoh H, Endo N, Sato R, Ikeshoji T, Matsuo M, et al. Density-functional study of perovskite-type hydride LiNiH 3 and its synthesis: mechanism for formation of metallic perovskite. Phys Rev B 2013;87:125134. https://doi.org/10.1103/PhysRevB.87.125134.
[33] Kresse G, Furthmüller J. Efficient iterative schemes for *ab initio* total-energy calculations using a plane-wave basis set. Phys Rev B 1996;54:11169–86. https://doi.org/10.1103/PhysRevB.54.11169.
[34] Kresse G, Furthmüller J. Efficiency of ab-initio total energy calculations for metals and semiconductors using a plane-wave basis set. Comput Mater Sci 1996;6:15–50. https://doi.org/10.1016/0927-0256(96)00008-0.
[35] Perdew JP, Burke K, Ernzerhof M. Generalized gradient approximation made simple. Phys Rev Lett 1996;77:3865–8. https://doi.org/10.1103/PhysRevLett.77.3865.
[36] Blöchl PE. Projector augmented-wave method. Phys Rev B 1994;50:17953–79. https://doi.org/10.1103/PhysRevB.50.17953.
[37] Kresse G, Joubert D. From ultrasoft pseudopotentials to the projector augmented-wave method. Phys Rev B 1999;59:1758–75. https://doi.org/10.1103/PhysRevB.59.1758.
[38] Pack JD, Monkhorst HJ. Special points for Brillouin-zone integrations;—a reply. Phys Rev B 1977;16:1748–9. https://doi.org/10.1103/PhysRevB.16.1748.
[39] Tang W, Sanville E, Henkelman G. A grid-based Bader analysis algorithm without lattice bias. J Phys Condens

Matter 2009;21:084204. https://doi.org/10.1088/0953-8984/21/8/084204.
[40] Bader RFW. Atoms in molecules : a quantum theory. Clarendon Press; 1990.
[41] Le Page Y, Saxe P. Symmetry-general least-squares extraction of elastic data for strained materials from *ab initio* calculations of stress. Phys Rev B 2002;65:104104. https://doi.org/10.1103/PhysRevB.65.104104.
[42] Togo A, Tanaka I. First principles phonon calculations in materials science. Scripta Mater 2015;108:1–5. https://doi.org/10.1016/J.SCRIPTAMAT.2015.07.021.
[43] Momma K, Izumi F, IUCr. *VESTA 3* for three-dimensional visualization of crystal, volumetric and morphology data. J Appl Crystallogr 2011;44:1272–6. https://doi.org/10.1107/S0021889811038970.
[44] Pan R-K, Yao J-G, Ji R-L, Liu W-W, Yin D-F. First principles study on elastic and electronic properties of bialkali alanates M2M′AlH6. Int J Hydrogen Energy 2018;43:3862–70. https://doi.org/10.1016/J.IJHYDENE.2018.01.006.
[45] Mouhat F, Coudert F-X. Necessary and sufficient elastic stability conditions in various crystal systems. Phys Rev B 2014;90:224104. https://doi.org/10.1103/PhysRevB.90.224104.
[46] Born M. On the stability of crystal lattices. I. Math Proc Cambridge Philos Soc 1940;36:160. https://doi.org/10.1017/S0305004100017138.
[47] Voigt W. Lehrbuch der Kristallphysik. Wiesbaden: Vieweg+Teubner Verlag; 1966. https://doi.org/10.1007/978-3-663-15884-4.
[48] Reuss A. Berechnung der fließgrenze von mischkristallen auf grund der plastizitätsbedingung für einkristalle. ZAMM - Zeitschrift Für Angew Math Und Mech 1929;9:49–58. https://doi.org/10.1002/zamm.19290090104.
[49] Hill R. The elastic behaviour of a crystalline aggregate. Proc Phys Soc 1952;65:349–54. https://doi.org/10.1088/0370-1298/65/5/307.
[50] Gencer A, Surucu G. Electronic and lattice dynamical properties of Ti_2SiB MAX phase. Mater Res Express 2018;5:076303. https://doi.org/10.1088/2053-1591/aace7f.
[51] Surucu G. Investigation of structural, electronic, anisotropic elastic, and lattice dynamical properties of MAX phases borides: an Ab-initio study on hypothetical M2AB (M = Ti, Zr, Hf; A = Al, Ga, In) compounds. Mater Chem Phys 2018;203:106–17. https://doi.org/10.1016/J.MATCHEMPHYS.2017.09.050.
[52] Pugh SF. XCII. Relations between the elastic moduli and the plastic properties of polycrystalline pure metals. Lond, Edinb, Dublin Philos Mag J Sci 1954;45:823–43. https://doi.org/10.1080/14786440808520496.
[53] Anderson OL. A simplified method for calculating the debye temperature from elastic constants. J Phys Chem Solids 1963;24:909–17. https://doi.org/10.1016/0022-3697(63)90067-2.
[54] Schreiber E, Anderson OL, Orson L, Soga N. Elastic constants and their measurement. McGraw-Hill; 1974.
[55] Miao N, Sa B, Zhou J, Sun Z. Theoretical investigation on the transition-metal borides with Ta3B4-type structure: a class of hard and refractory materials. Comput Mater Sci 2011;50:1559–66. https://doi.org/10.1016/J.COMMATSCI.2010.12.015.
[56] Gaillac R, Pullumbi P, Coudert F-X. ELATE: an open-source online application for analysis and visualization of elastic tensors. J Phys Condens Matter 2016;28:275201. https://doi.org/10.1088/0953-8984/28/27/275201.
[57] Clarke DR, Levi CG. Materials design for the next generation thermal barrier coatings. Annu Rev Mater Res 2003;33:383–417. https://doi.org/10.1146/annurev.matsci.33.011403.113718.
[58] Cahill DG, Watson SK, Pohl RO. Lower limit to the thermal conductivity of disordered crystals. Phys Rev B 1992;46:6131–40. https://doi.org/10.1103/PhysRevB.46.6131.
[59] Zeng Q, Su K, Zhang L, Xu Y, Cheng L, Yan X. Evaluation of the thermodynamic data of CH3SiCl3 based on quantum chemistry calculations. J Phys Chem Ref Data 2006;35:1385–90. https://doi.org/10.1063/1.2201867.
[60] Bourgeois N, Crivello J-C, Cenedese P, Joubert J-M. Systematic first-principles study of binary metal hydrides. ACS Comb Sci 2017;19:513–23. https://doi.org/10.1021/acscombsci.7b00050.